Jordan Journal of Civil Engineering, Volume **2**, No. **2**, **2008**

Non-Linear Seismic Response of Base-Isolated Frame Structures Using Rubber Bearings

Anis S. Shatnawi[1)], Abdelqader S. Najmi[2)], Mu'tasim S. Abdel-Jaber[1)] and Iyad M. Amareen[3)]

[1)] Assistant Professor, Department of Civil Engineering, The University of Jordan
(Corresponding Author: ashatnawi@ju.edu.jo)
[2)] Professor, Department of Civil Engineering, The University of Jordan
[3)] MSc Student, Department of Civil Engineering, The University of Jordan

ABSTRACT

Over the past two decades, much progress has been made in research and application of the base isolation of structures as means of providing earthquake resistance to a structure. However, the trade-off between the extent of acceleration reduction and the response of a base-isolation system has not been given a serious consideration. This work uses a new material constitutive model for rubber bearing base-isolation system, which adopts the technique of real-time structural parameter modification. To achieve this, a finite element modeling and analysis are performed as a comparative study between a conventional totally fixed-base steel frame structure and similar base-isolated structures using rubber-steel bearings. The structures are subjected to the El-Centro, N-S earthquake.

In order to include nonlinearity effects, a non-linear hyperviscoelastic material model has been used and linked to ABAQUS software as a user defined material subroutine (i.e., UMAT). Special connector elements are selected from ABAQUS library to connect the rubber bearings to the frame structure and the foundations in order to achieve the required kinematical constraints at the connection points. The model is validated by carrying out a comparative study of the results obtained from the analysis of the presented material model with those obtained by using the existing ABAQUS material models (e.g., Ogden material model). The results show a significance efficiency of using the rubber bearing isolation in order to uncouple the structure from the seismic ground motion. Moreover, it has been proved that the used material model is more effective to capture the behavior of the base-isolated structures expressing a notable reduction in acceleration and an increase in the structural resistance to earthquake excitations.

KEYWORDS: Rubber-steel bearing, Hyperelasticity, Base isolation, Direct integration.

INTRODUCTION

Historically, major earthquakes caused damage to civil engineering structures in different regions of the world (Yefim, 1999). The non-linear response of structures subjected to earthquake excitations has been a vital issue that worries engineers and researchers.

Salomon et al. (1999) introduced an analytical and numerical model for a high damping rubber bearing that took into account the highly nonlinear elastic behavior of the rubber bearing and its energy dissipation. The Ogden strain energy function was used in the analysis. Also, the model was confirmed by comparing with existing experimental results. A few years later, Carrillo (2005)

Accepted for Publication on 1/4/2008.

presented a case study on the effect of inserting high damping rubber bearings as a base isolation system to a symmetrical, low-rise reinforced concrete structure in Algeria. He found that although base isolators are expensive, they reduce the acceleration effectively. Also, they reduce the quantity of steel needed in design significantly. In addition to these studies, Hwang et al. (2002) presented a mathematical hysteretic model for elastomeric isolation bearings that was validated by material tests and the shaking table test. The model was capable of predicting the shear force-displacement hysteresis very accurately for both rubber material and bearing under cyclic loading reversals.

In order to study the seismic response of the rubber-steel bearings, a non-linear material constitutive model for large strain has been used and linked to the ABAQUS software as a user-defined material model subroutine (i.e., UMAT) obtained from the study of Al-Shatnawi (2001). This model has been verified and checked against existing hyperelastic material models found within ABAQUS (e.g., Ogden model). The rubber material is assumed to be isotropic with a non-linear elastic behavior (i.e., hyperelastic behavior).

A non-linear two-dimensional based seismic analysis that includes nonlinear material and geometric effects is also performed using ABAQUS software for base-isolated frame structures using rubber-steel bearings when subjected to El-Centro, N.S. earthquake (Fig. 1). The focus will be on investigating the response of base-isolated low-rise (Fig. 2) and high-rise (Fig. 3) steel structures along with the response of the rubber bearing system (Fig. 4 and Fig. 5) that was used to isolate the high-rise frame model itself. In order to connect the rubber bearings to the steel frame, a WELD connection type is used and the results obtained are confirmed using the TIE constraints.

The elements CPS4R and B21 which are available in ABAQUS were used to develop the mesh representation for the rubber bearing's elements and the frame elements, respectively. In addition, very fine meshes were used to obtain more accurate results.

FORMULATION

Large Deformation Mechanics

In order to define large deformation strain measure, the relationship between the initial and deformed configurations of the body (Fig. 6) must be defined by vector addition as follows:

$$x_i = X_i + u_i \tag{1}$$

where x_i and X_i are the position vectors in the initial and deformed configurations, respectively; while u_i is the displacement.

The derivation of Equation (1) with respect to *X* leads to

$$\frac{\partial x_i}{\partial X_j} = \frac{\partial X_i}{\partial X_j} + \frac{\partial u_i}{\partial X_j} \tag{2}$$

where $\frac{\partial X_i}{\partial X_j}$ is a second order identity tensor. It can be represented by the Kronecker delta as:

$$\frac{\partial X_i}{\partial X_j} = \delta_{ij} \tag{3}$$

The material orientation vectors must also be defined in both initial and deformed configurations by using the finite element method mapping technique using the chain rule in Equation (1) as follows:

$$dx_i = \frac{\partial x_i}{\partial X_j} \partial X_j \tag{4}$$

$\frac{\partial x_i}{\partial X_j}$ is defined as the deformation gradient tensor and can be written as:

$$F_{ij} = \frac{\partial x_i}{\partial X_j} \tag{5}$$

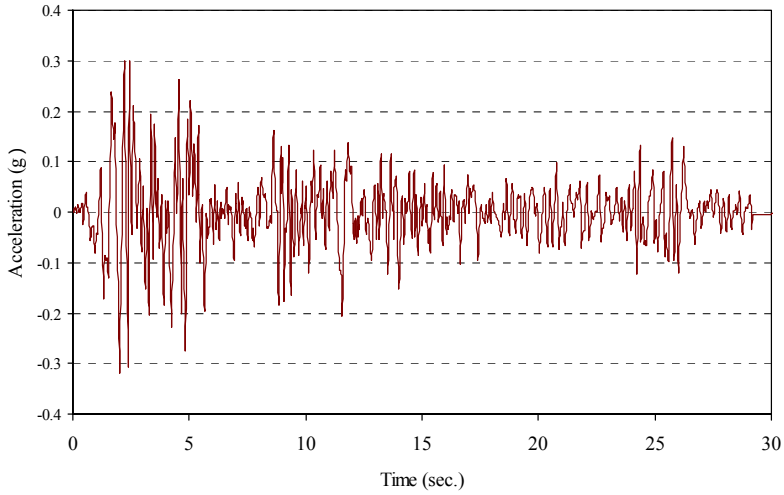

Fig. (1): Input ground acceleration of El-Centro, N-S earthquake.

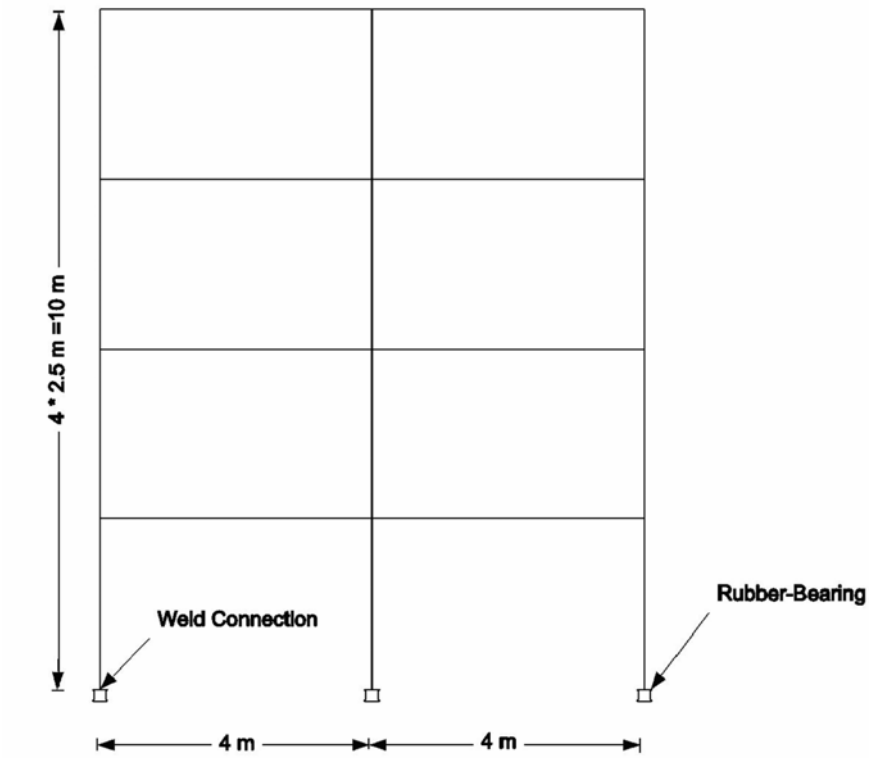

Fig. (2): Base-isolated low-rise steel frame model.

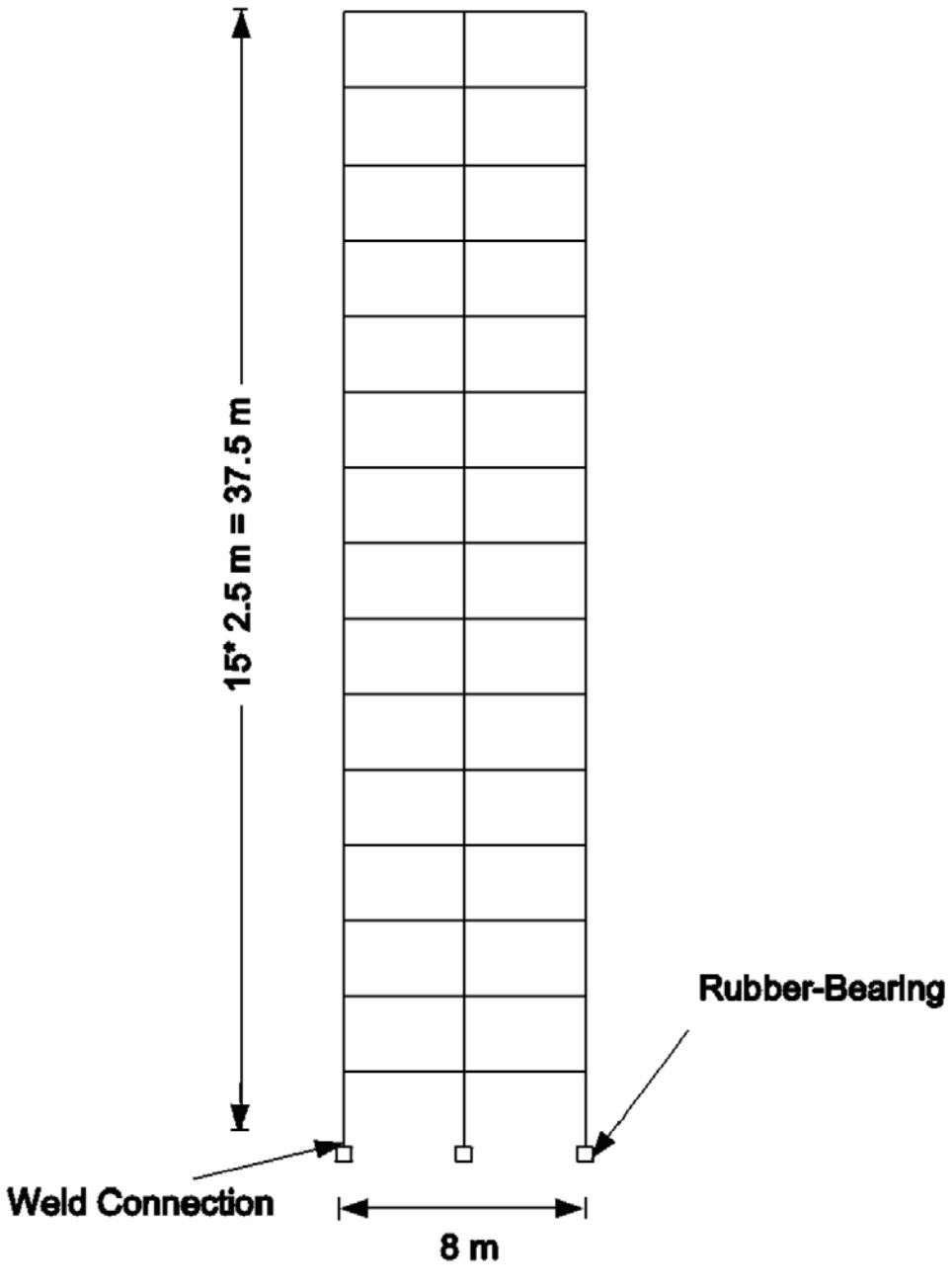

Fig. (3): Base-isolated high-rise steel frame model.

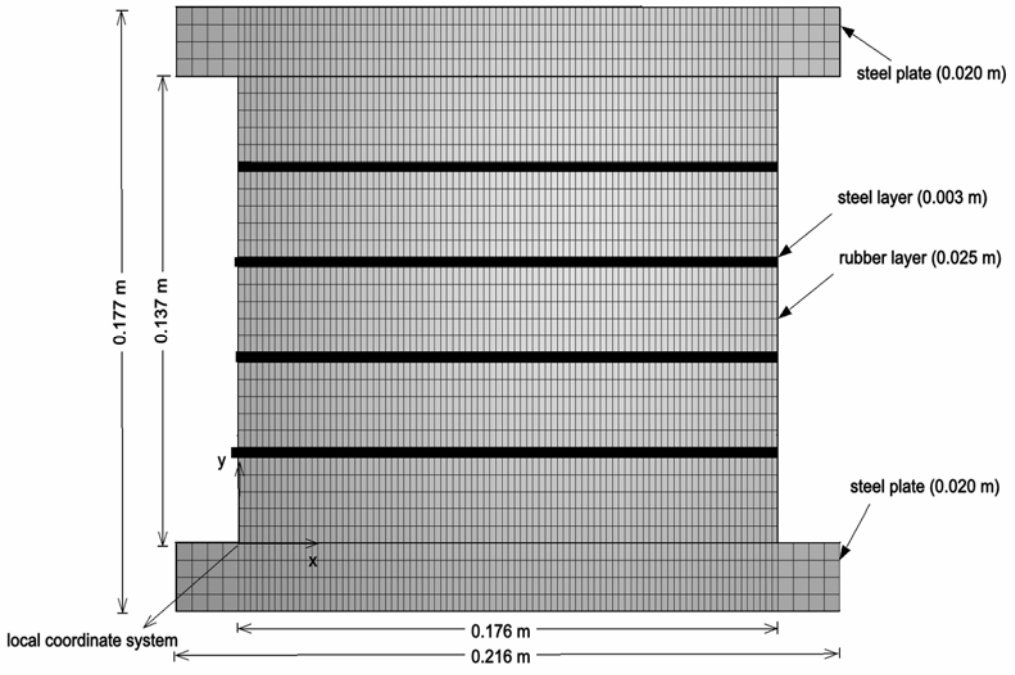

Fig. (4): Rubber-steel bearing used for isolating the low-rise frame model.

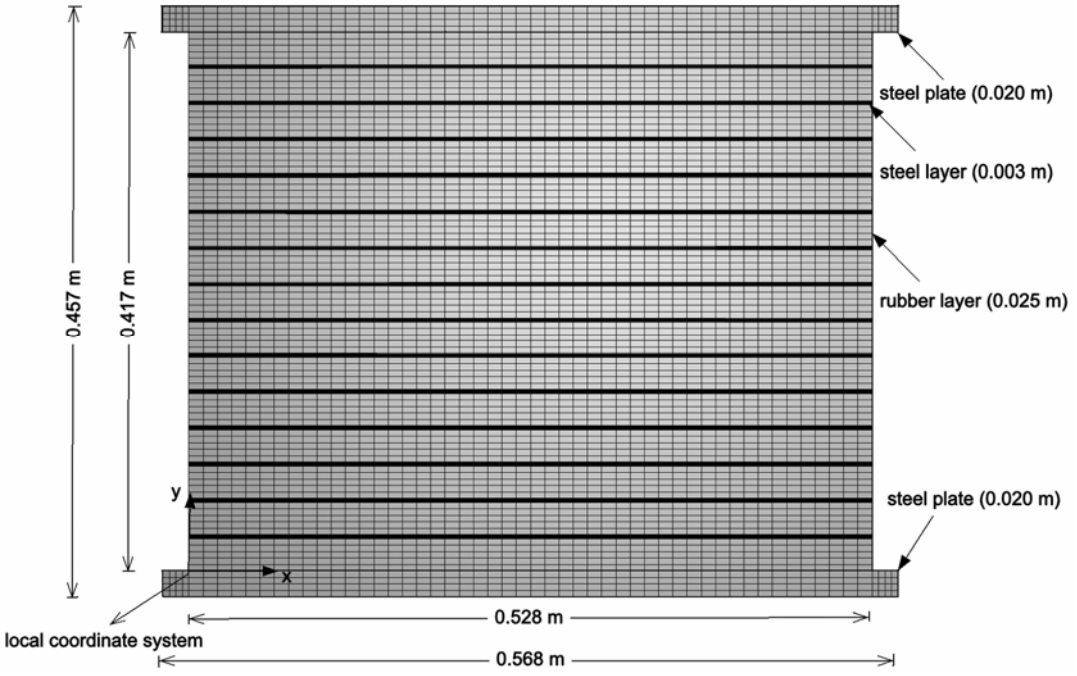

Fig. (5): Rubber-steel bearings used for isolating the high-rise frame model.

By substituting Equations (3) and (4) in Equation (2), it becomes:

$$F_{ij} = \delta_{ij} + \frac{\partial u_i}{\partial X_j} \tag{6}$$

In order to define a strain measure that is independent of the rigid body motion and rotation, the change in length squared in a material vector when going from the initial configuration to the deformed one must be measured.

The length squared could be written for the initial configuration as:

$$(ds')^2 = dX_i dX_i \tag{7}$$

For the final configuration:

$$(ds)^2 = dx_i dx_i \tag{8}$$

$$(ds')^2 - (ds)^2 = dX_i dX_i - dx_i dx_i = 2dX_i E_{ij} dX_j \tag{9}$$

where E_{ij} is the strain tensor.

Replacing dX by the deformation gradient tensor definition will reform the above equation into the following shape:

$$dx_i F_{ki} F_{kj} dx_j - dx_i dx_i = 2dX_i E_{ij} dX_j \tag{10}$$

Note that the following holds:

$$\underbrace{dx_i F_{ki}}_{dX_k} \underbrace{F_{kj} dx_i}_{dX_k} = dX_i dX_i = dX_i \delta_{ij} dX_j \tag{11}$$

Substituting the second and third terms of Equation (11) in the strain equation, it becomes:

$$dX_i F_{ki} F_{kj} dX_j - dX_i \delta_{ij} dX_j = dX_i (F_{ki} F_{kj} - \delta_{ij}) dX_j = 2dX_i E_{ij} dX_j \tag{12}$$

From which the strain **E** could be written in terms of the deformation gradient tensor as:

$$E_{ij} = \frac{1}{2}(F_{ki} F_{kj} - \delta_{ij}). \tag{13}$$

The right Cauchy deformation tensor C_{ij} is defined as:

$$C_{ij} = F_{ki} F_{kj} \tag{14}$$

The Green-Lagrange strain tensor could be written in terms of the right Cauchy deformation tensor as:

$$E_{ij} = \frac{1}{2}(C_{ij} - \delta_{ij}) \tag{15}$$

Hyperelasticity

Decomposing the gradient deformation tensor, **F**, the right Cauchy tensor, **C** and the Lagrangian strain tensor, **E** will result in the following equations:

$$\mathbf{F} = J^{1/3}\,\hat{\mathbf{F}} \tag{16a}$$

$$\hat{\mathbf{C}} = J^{-2/3}\,\mathbf{C} = \hat{\mathbf{F}}^{\mathbf{T}}\hat{\mathbf{F}} \tag{16b}$$

$$\hat{\mathbf{E}} = \frac{1}{2}(\hat{\mathbf{C}} - \mathbf{I}) \tag{16c}$$

where $\hat{\mathbf{F}}$ is the isochoric distortional deformation ($\det\hat{\mathbf{F}}=1$), $J^{1/3}\mathbf{I}$ is the pure dilatation and $\hat{\mathbf{C}}$ is the modified, volumetric preserving deformation tensor (Saleeb et al., 1992; Hughes, 1998). Now, knowing that $\mathbf{I}^{(4)}$ is the unit tensor, one can write:

$$I^{(4)}_{ijkl} = \frac{1}{2}(\delta_{ik}\delta_{jl} + \delta_{il}\delta_{jk}) \tag{17}$$

Next is representing the hyperelastic material by a strain energy function where Ogden model is adopted. The deviatoric part of the stored-energy function can be defined as:

$$\hat{W} \equiv \hat{W}(\hat{\lambda}_i) = \sum_{n=1}^{N} \frac{a_n}{\alpha_n}(\hat{\lambda}_1^{\alpha_n} + \hat{\lambda}_2^{\alpha_n} + \hat{\lambda}_3^{\alpha_n} - 3) \tag{18}$$

where $\hat{\lambda}$ are the principal values of $\hat{\mathbf{C}}$.

a_n and α_n are material constants.

IMPLICIT DYNAMIC ANALYSIS USING DIRECT INTEGRATION

Hilber-Hughes-Taylor operator which is an implicit method extended from the trapezoidal rule is the general direct integration method used by ABAQUS to perform the analysis. This is done by solving a set of simultaneous equations iteratively using Newton's method.

The equilibrium equation could be written using the finite element approximation as follows:

$$M^{NM}\ddot{u}^{M} + I^{N} - P^{N} = 0 \quad (19)$$

Note that

M^{NM} : Consistent mass matrix
I^{N} : Internal force vector
P^{N} : External force vector
$\ddot{u}^{M}$: Acceleration

The implicit operator defined by Hilber and Hughes is used for time integration of the dynamic problem. It replaces the equilibrium equation with the following equation:

$$M^{NM}\ddot{u}^{M}\big|_{t+\Delta t} + (1+\alpha)(I^{N}\big|_{t+\Delta t} - P^{N}\big|_{t+\Delta t}) - \alpha(I^{N}\big|_{t} - P^{N}\big|_{t}) + L^{N}\big|_{t+\Delta t} = 0 \quad (20)$$

where $L^{N}\big|_{t+\Delta t}$ is the sum of all Lagrange multiplier forces associated with degree of freedom N and α is a damping control parameter.

The operator definition is completed by the Newmark formulae for displacement and velocity integration:

$$u\big|_{t+\Delta t} = u\big|_{t} + \Delta t\,\dot{u}\big|_{t} + \Delta t^{2}((\frac{1}{2}-\beta)\ddot{u}\big|_{t} + \beta\ddot{u}\big|_{t+\Delta t}) \quad (21)$$

and

$$\dot{u}\big|_{t+\Delta t} = \dot{u}\big|_{t} + \Delta t((1-\gamma)\ddot{u}\big|_{t} + \gamma\ddot{u}\big|_{t+\Delta t}) \quad (22)$$

where u, $\dot{u}$ and $\ddot{u}$ are the displacement, velocity and acceleration, respectively, while Δt is the time increment.

$$\beta = \frac{1}{4}(1-\alpha)^{2}, \quad \gamma = \frac{1}{2} - \alpha \quad \text{and} \quad -\frac{1}{3} \le \alpha \le 0 \quad (23)$$

Damping is considered here using the artificial damping. Artificial damping is controlled through the numerical damping control parameter; $\tilde{\alpha}$.

Implicit dynamic analysis is expensive especially in time and hard work. However, it is one of the most suitable methods in dealing with nonlinear dynamic problems.

RESULTS AND DISCUSSION

Rubber-Steel Bearing Models and Verification

Figs. 7 and 8 show the stresses distribution (σ_{11} and σ_{22}, respectively) along the elements at the bottom of the lower steel plate when ABAQUS/STANDARD large strain model was used in expressing the rubber material. They are compared to the stresses distribution (σ_{11} and σ_{22}, respectively) along the same elements when the hyperviscoelastic material model was implemented and used as a user-defined material subroutine in ABAQUS (i.e., UMAT). In order to validate the results obtained for the rubber material when dealing with stresses, they are both plotted at the time of maximum acceleration (i.e., 2.02 seconds). The results obtained showed identical behavior and good agreement when using either the ABAQUS/Standard model or when using the user-defined material subroutine (i.e., UMAT).

Figs. 9 and 10 show the horizontal acceleration and displacement of the upper right node of the rubber bearing model versus time. Both figures show good agreement when using either the Ogden model of ABAQUS or the proposed hyperviscoelastic model implemented as a user-defined material subroutine (i.e., UMAT).

Lateral force is plotted against the lateral displacement in Fig. 11 for a node located at the upper-right corner of the rubber-steel bearing model. The results obtained showed identical behavior when using either the ABAQUS/Standard model or the user-defined material subroutine (i.e., UMAT).

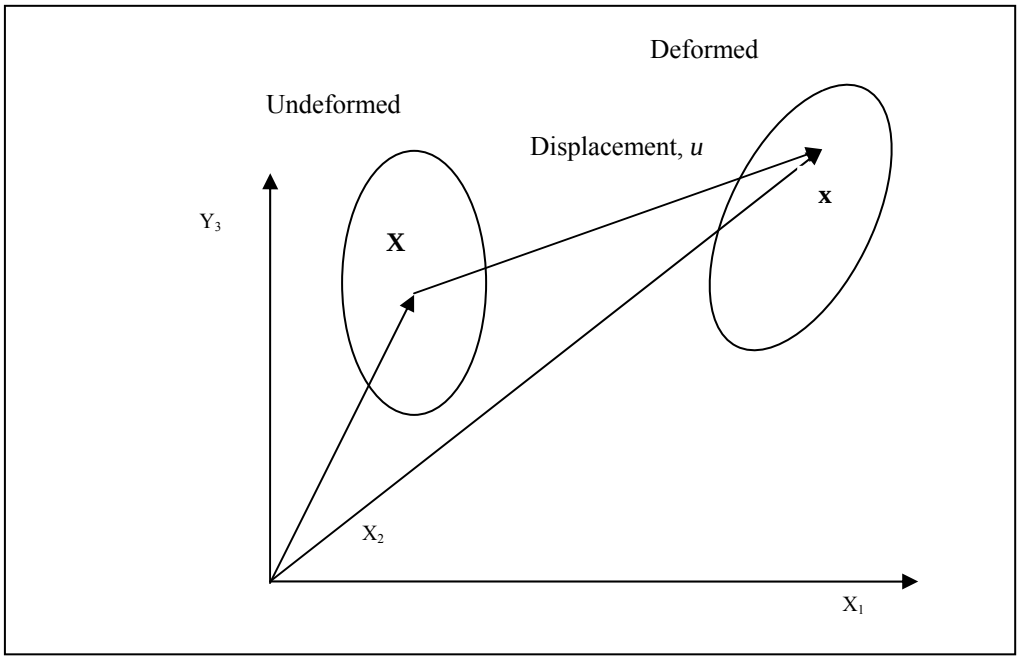

Fig. (6): Relationship between the initial and deformed configurations of the body.

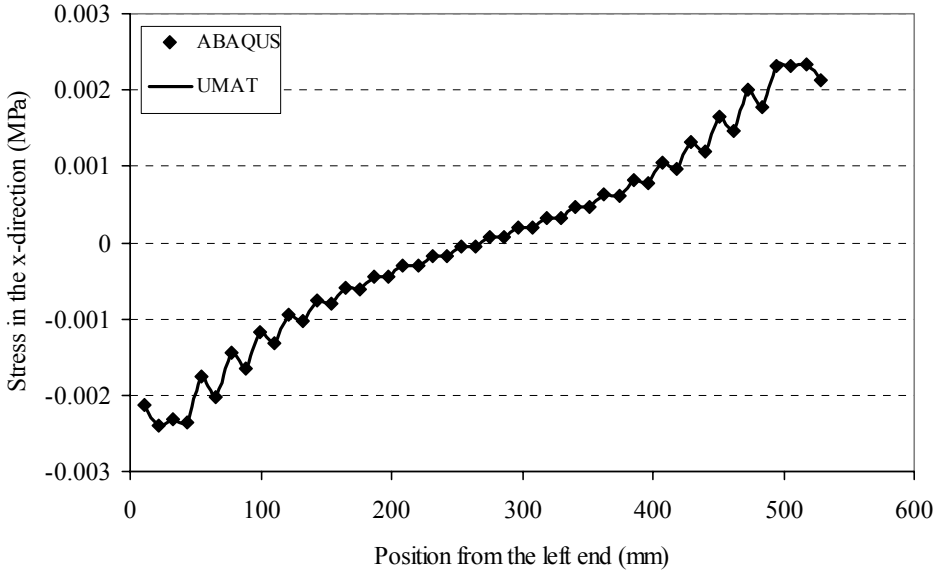

Fig. (7): Stress in the x-direction versus the position from the left end at the bottom of the rubber-steel bearing.

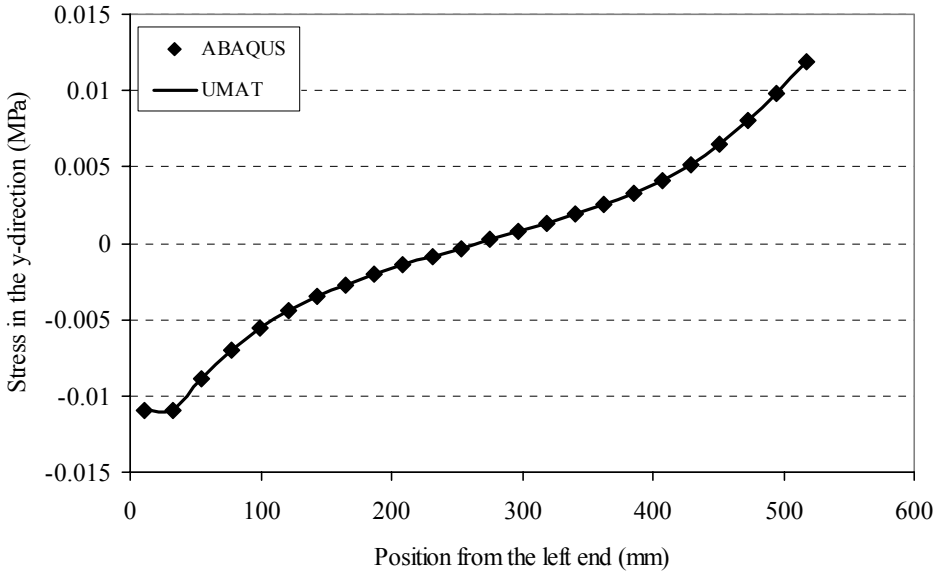

Fig. (8): Stress in the y-direction versus the position from the left end at the bottom of the rubber-steel bearing.

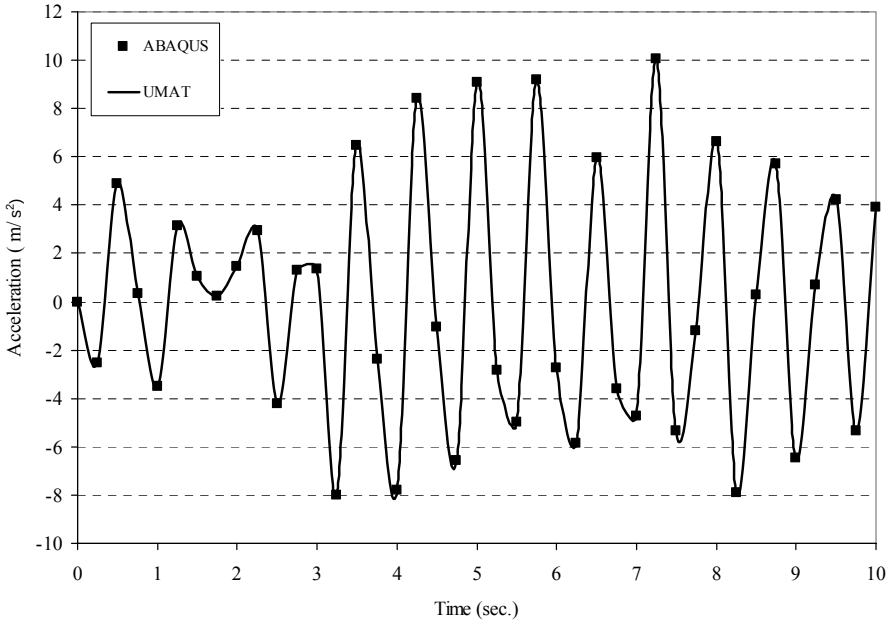

Fig. (9): Horizontal acceleration versus time of a node located at the upper-right corner of the rubber-steel bearing.

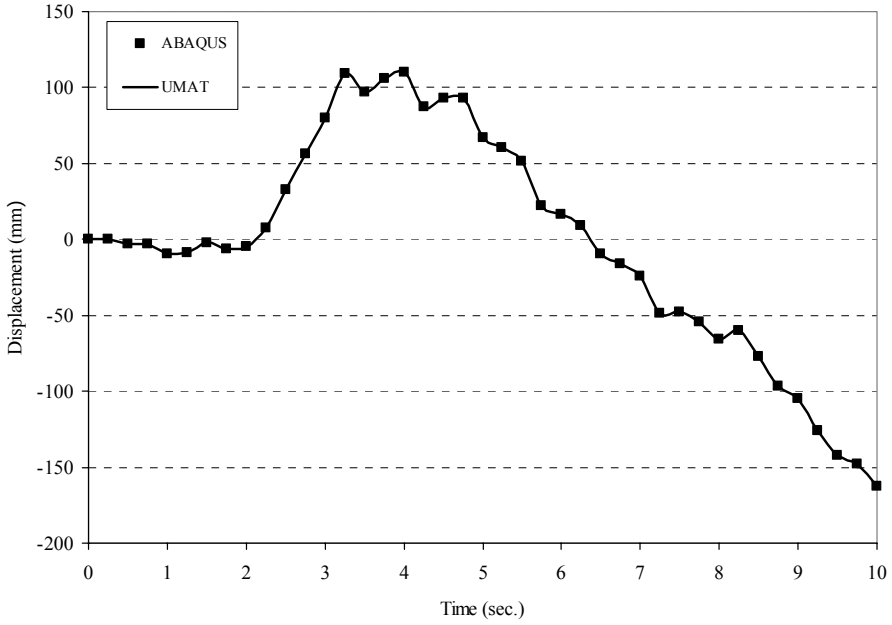

Fig. (10): Horizontal displacement versus time of a node located at the upper-right corner of the rubber-steel bearing.

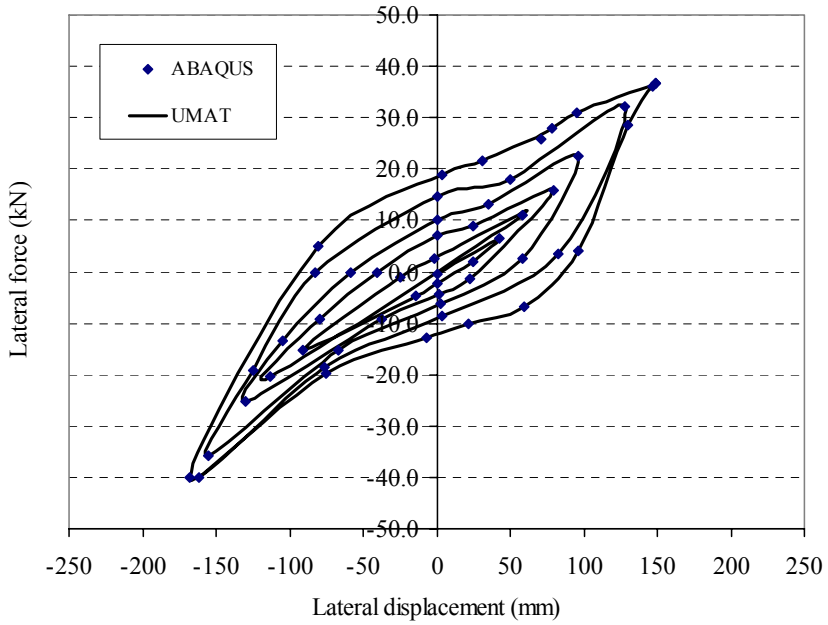

Fig. (11): Lateral force versus the lateral displacement for a node located at the upper right corner of the rubber-steel bearing model.

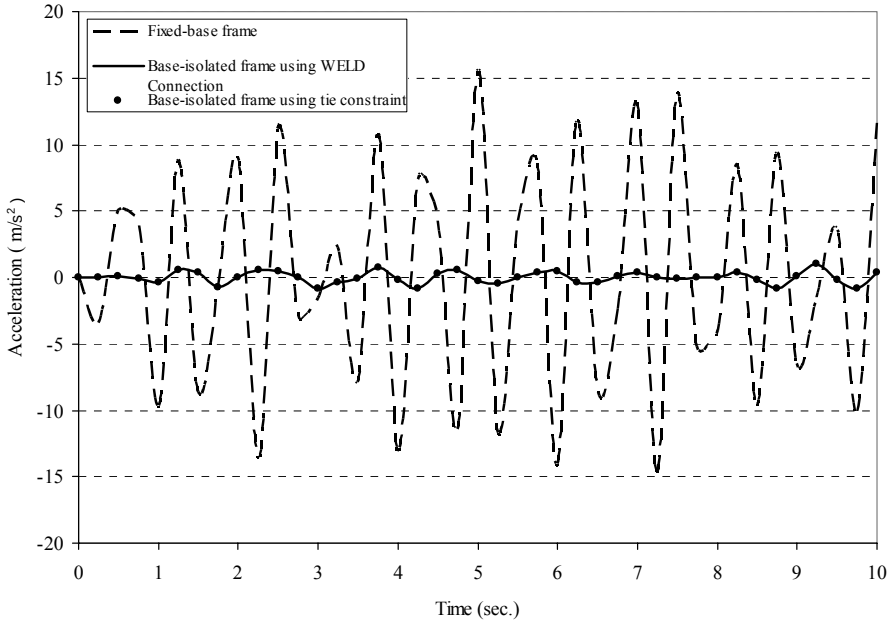

Fig. (12): Horizontal acceleration versus time for a node located at the upper-right corner of the fixed-base and base-isolated low-rise frame models.

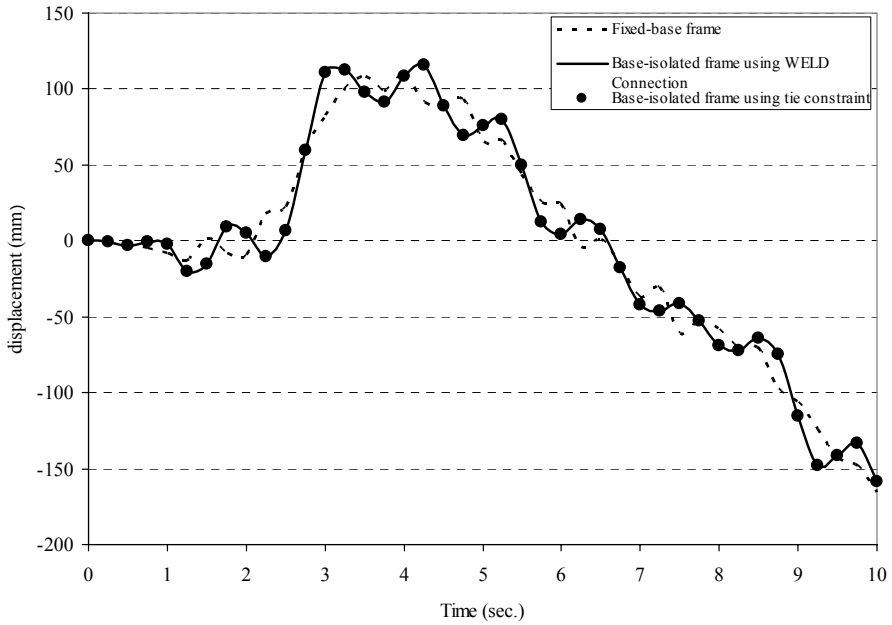

Fig. (13): Horizontal displacement versus time for a node located at the upper-right corner of the fixed-base and base-isolated low-rise frame models.

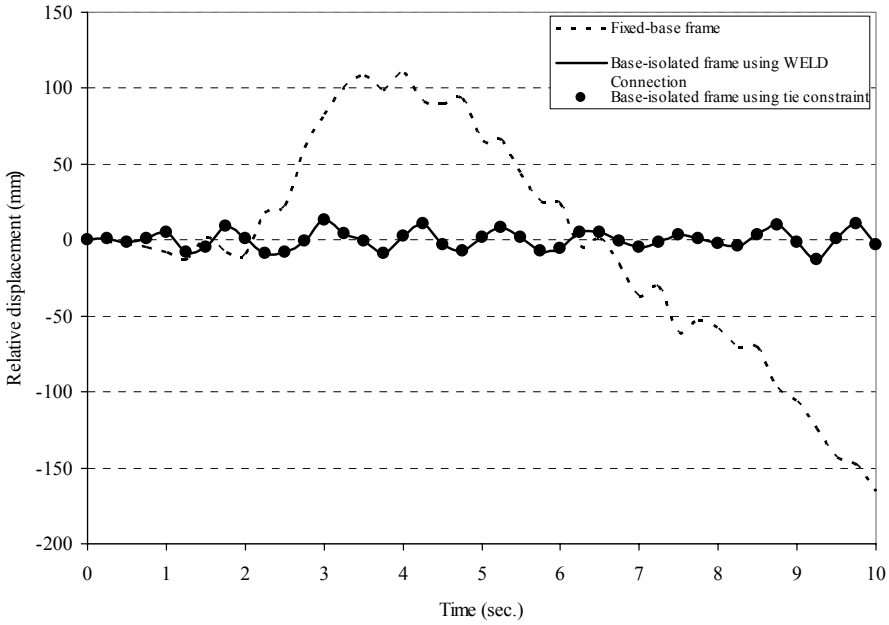

Fig. (14): Relative displacement versus time of a node located at the upper-right corner of the fixed-base and base-isolated low-rise frame models.

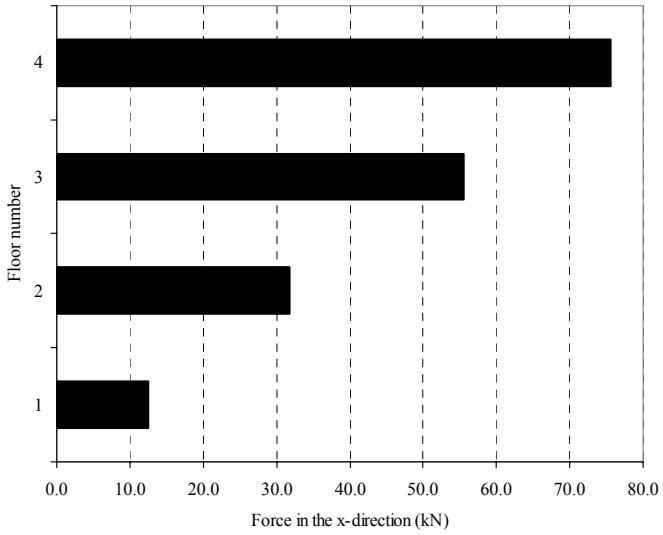

Fig. (15): The floor number versus the horizontal force for the fixed-base low-rise frame model.

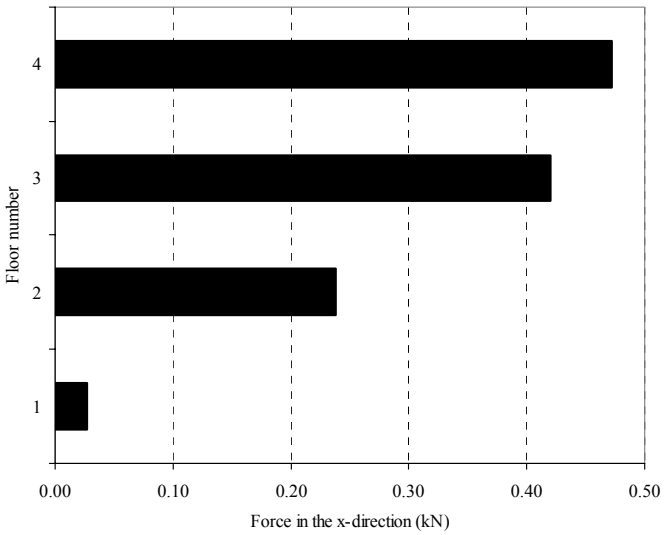

Fig. (16): The floor number versus the horizontal force for the base-isolated low-rise frame model.

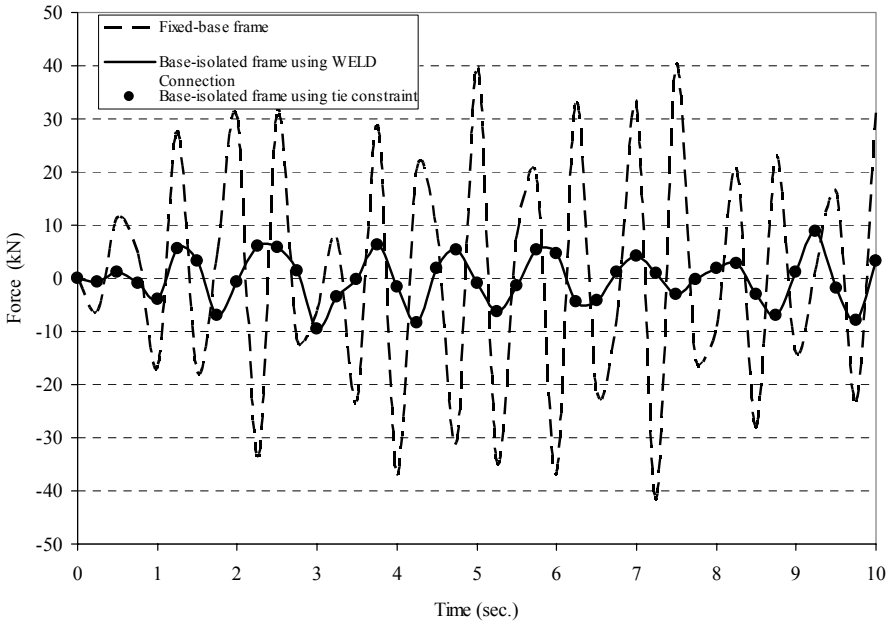

Fig. (17): Reaction force in the x-direction versus time for a node located at the lower-right corner of the fixed-base and base-isolated low-rise frame models.

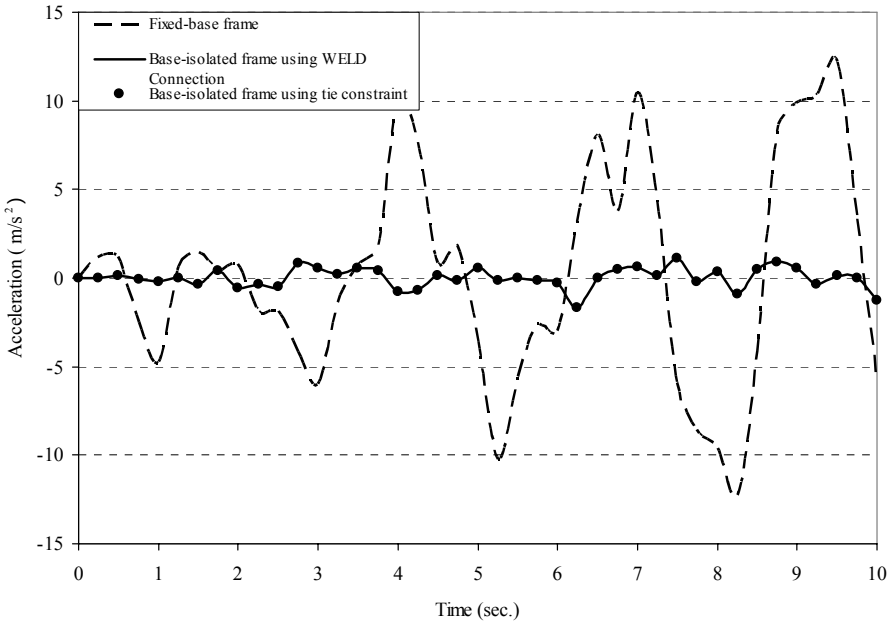

Fig. (18): Horizontal acceleration versus time for a node located at the upper-right corner of the fixed-base and base-isolated high-rise frame models.

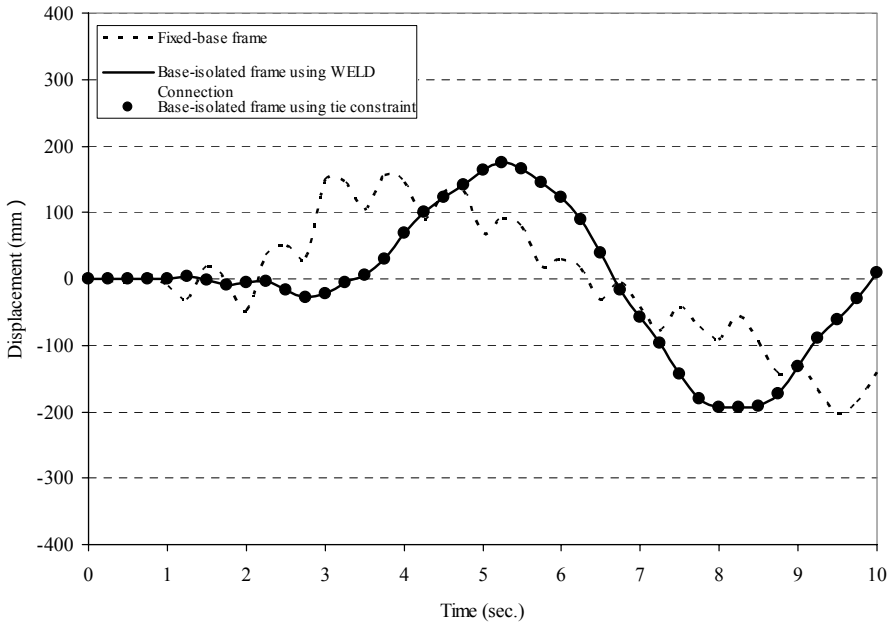

Fig. (19): Horizontal displacement versus time for a node located at the upper-right corner of the fixed-base and base-isolated high-rise frame models.

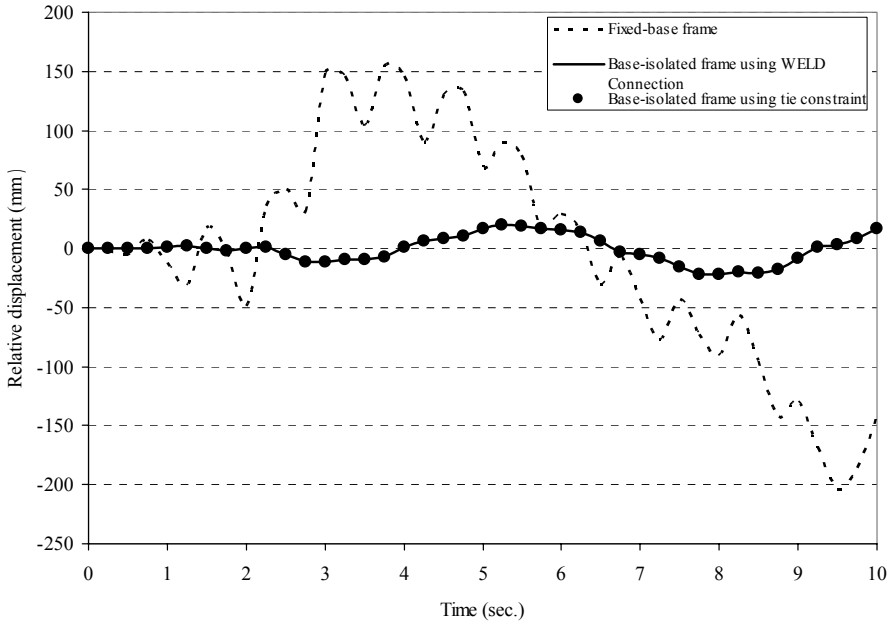

Fig. (20): Relative displacement versus time of a node located at the upper-right corner of the fixed-base and base-isolated high-rise frame models.

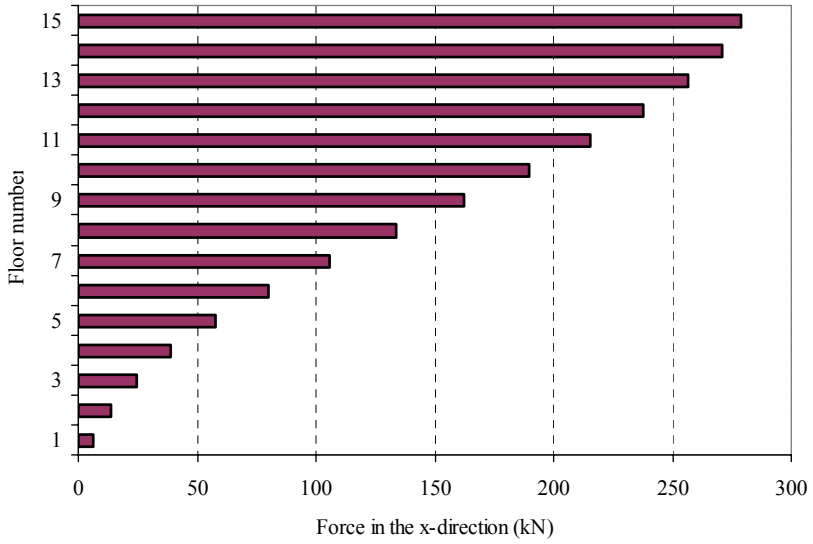

Fig. (21): The floor number versus the horizontal force for the fixed-base high rise frame model.

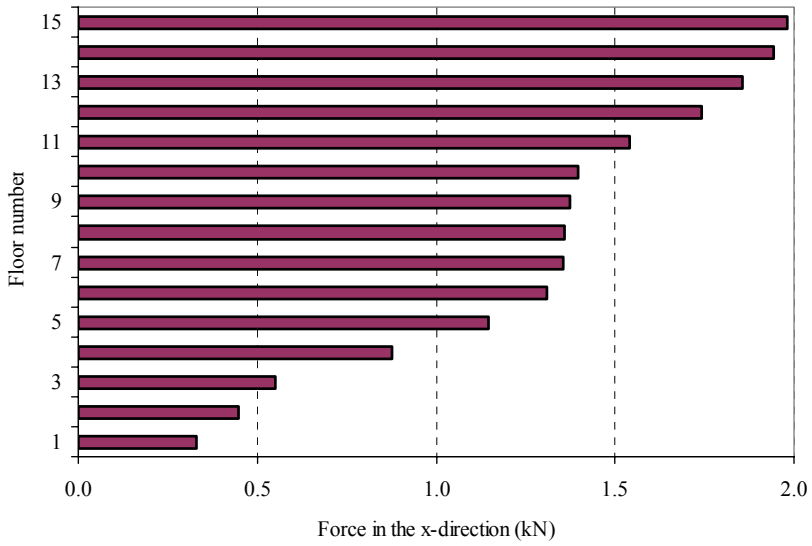

Fig. (22): The floor number versus the horizontal force for the base-isolated high-rise frame model.

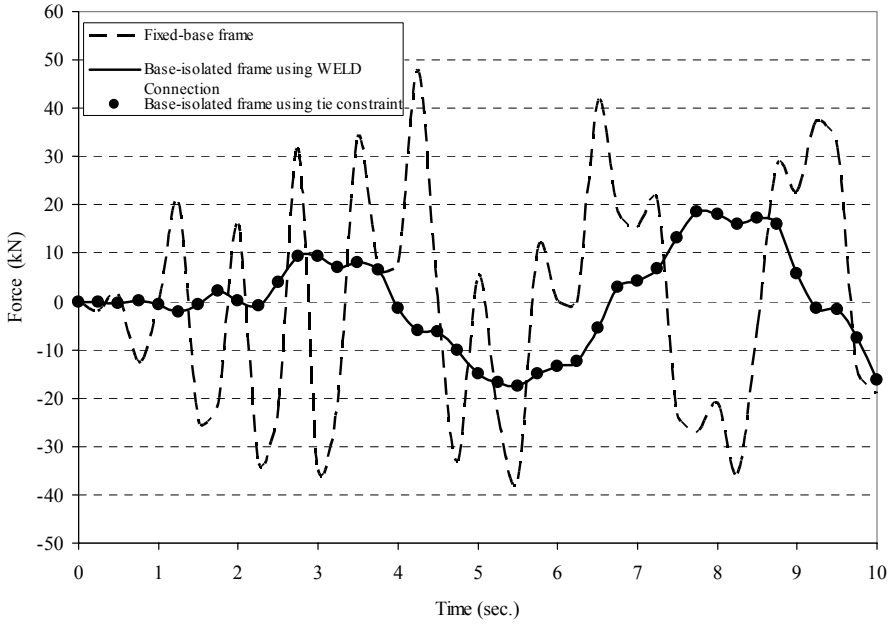

Fig. (23): Reaction force in the x-direction versus time for a node located at the lower-right corner of the fixed-base and base-isolated high-rise frame models.

Table 1. Material parameters of the rubber-steel bearings used to isolate the low-rise and high-rise frame models.

Property	Low-rise frame values	High-rise frame values
Modulus of Elasticity (E) (N/m^2)	198.252E9	198.252E9
Steel's Poisson ratio	0.2273	0.2273
Density (kg/m^3)	7800	7800

Table 2. Geometrical properties of the rubber-steel bearing used to isolate the low-rise and high-rise frame models.

Property	Low-rise frame values	High-rise frame values
Number of rubber layers	5	15
Number of steel layers	4	14
Thickness of each rubber layer (m)	0.025	0.025
Thickness of each steel sheet (m)	0.003	0.003
Thickness of end steel plates (m)	0.020	0.020

Table 3. Geometrical properties of beams and columns of the low-rise frame model.

Property		Columns	Beams
Section type		Box	Box
Section Dimensions (*m*)	Width	0.35	0.20
	Height	0.35	0.25
	Thickness	0.04	0.025
Modulus of Elasticity, ***E***, (*Pa*)		200E9	200E9
Poisson ratio		0.25	0.25
Density (kg/m^3)		7800	7800

Table 4. Geometrical properties of beams and columns of the high-rise frame model.

Property		Columns	Beams
Section type		Box	Box
Section Dimensions (*m*)	Width	0.50	0.20
	Height	0.50	0.25
	Thickness	0.04	0.025
Modulus of Elasticity, ***E***, (*Pa*)		200E9	200E9
Poisson ratio		0.25	0.25
Density (kg/m^3)		7800	7800

Low-Rise and High-Rise Frame Models

Floor acceleration plays a significant role in increasing or decreasing the damage to the building installation. Decreasing the acceleration decreases the damage of the structural members. In Fig. 12, and in order to investigate the effect of inserting the rubber-steel bearings on the behavior of the low-rise frame model when it is subjected to the El-Centro, N-S earthquake, the horizontal acceleration of the upper right node in the low-rise isolated frame is plotted versus time. Then, it is compared to the horizontal acceleration of the same node when the frame is totally fixed without using rubber bearings. The figure shows a high efficiency of using the rubber-steel bearing in reducing the acceleration over time and elongating the building's period.

Fig. 13 shows the horizontal displacement versus time of the upper-right node in the low-rise base-isolated frame. It is compared to the horizontal displacement of the same node when the frame is totally fixed. From the figure, it is seen that the maximum horizontal displacement has not been affected much. However, its variation over time decreased slightly when using the rubber bearings. Consequently, the period was elongated slightly when the frame was isolated.

Relative displacement is an important parameter in measuring the structural damage. As the relative displacement decreases, less structural damage occurs. In Fig. 14, relative displacement of the upper right node in the low-rise isolated frame is plotted over time. Then, it is compared to the relative displacement of the same node when the frame is totally fixed without rubber bearings. It is clearly seen that isolating the low-rise frame model helped in decreasing the relative horizontal displacement efficiently. Moreover, the period was elongated when the isolation system was used leading to less structural damage.

Figs. 15 and 16 show the horizontal force plotted against the floor number at the right side of the frame for the low-rise fixed-base and the low-rise base-isolated frames, respectively. From both Figures, it is seen that the horizontal forces at higher floors is much higher than the horizontal forces at lower floors. Moreover, the horizontal forces decrease when the high-rise frame is base-isolated. This shows the good effect of using the rubber-steel bearing isolation in reducing the lateral forces acting on the structure.

In Fig. 17, the reaction force in the horizontal direction at the right side base node in the low-rise base-isolated frame is compared to the reaction force in the horizontal direction of the same node when the frame is totally fixed without using rubber bearings. They are both plotted over time. It is clear that using the rubber-steel bearings gives excellent effect in reducing the reaction force. Reaction force in the x-direction dropped significantly over the entire time.

The behavior of the high-rise frame model was similar to the behavior of the low-rise frame model when the rubber bearings were used to isolate both frames. This is clearly seen when analyzing Figs. 18 to 23 which represent the results obtained for the high-rise frame model regarding the acceleration, displacement, relative displacement, floor number versus the horizontal force and the reaction force versus time. However, the behavior of both frames was different when considering some other factors. For example, although the horizontal displacement did not change much when both frames were isolated, the period of the high-rise frame was relatively more elongated.

Using either the WELD connection or the tie constraint for isolating the low-rise frame model gave identical results for the horizontal acceleration, horizontal displacement, relative displacement, floor number versus the horizontal force, lateral force versus the lateral displacement and the reaction force in the x-direction versus time. This validates the results obtained for those types of connections.

CONCLUSIONS

In the study, the response of the rubber-steel bearing isolation system has been considered and studied separately, and the material models of the rubber were investigated and verified. Moreover, the non-linear seismic responses of a fixed-base and base-isolated steel frame structures were analyzed.

The stresses, accelerations and displacements of the rubber bearing system were computed using two material models. These are: a hyperviscoelastic material model (Al-Shatnawi, 2001) that is linked with ABAQUS as a user defined material model (UMAT), and another large strain hyperelastic material model that exists within the ABAQUS software (i.e., Ogden type). Based on modified material model, when the structure is subjected to El-Centro, N-S earthquake, the stresses, acceleration history, lateral displacements and the lateral forces versus the lateral displacements of the rubber bearings are all found to have good agreement with those obtained when using the hyperelastic Ogden model of ABAQUS.

Moreover, similar responses of the fixed-base and base-isolated steel frames regarding the relative floor displacements, accelerations and some other factors are obtained and found to be in good agreement using either the WELD connection or the TIE constraint to represent the kinematic constraints at the connection point between the rubber-bearings and the frames.

Rubber-bearings showed a great efficiency in uncoupling both structures from the seismic ground motion helping both of them to sustain the earthquake excitation. This is observed by elongating the period of the structure and reducing the horizontal accelerations, lateral-forces and the relative horizontal roof displacement. However, better results are observed for the high-rise structures, because their period increased relatively more than the period of the low-rise structures which reduced the effect of the earthquake excitation on this type of structures and led to less structural damage.

REFERENCES

ABAQUS. 2003. Analysis User's Manual, Ver. 6.4, Hibbitt, Karlsson and Sorensen, Inc.,

Al-Shatnawi, A. 2001. Developments for Complex Inelastic Large-scale Simulations and Parameter Estimation, with emphasis on Large Strain, Softening and Localization Phenomena, PhD Dissertation, University of Akron.

Amareen, Iyad. 2007. Non-linear Seismic Response of Base-isolated Frame Structures Using Rubber Bearings, Master Thesis, Department of Civil Engineering, The University of Jordan.

Carrillo, Abiel. 2005. Seismic Isolation for Small Reinforced Concrete Structures: A Preliminary Investigation on Material Cost. Master Thesis, New Mexico State University, at State University of New York at Buffalo, Advised and Supervised by Dr. George C. Lee.

Chopra, A. K. 1995. Dynamic of Structures, Linköping Institute of Technology, Sweden.

Clough, R. and Penzien, J. 1993. Dynamics of Structures, McGraw-Hill, Inc, Singapore.

Gendy, A.S. and Saleeb, A.F. 2000. Nonlinear Material Parameter Estimation for Characterizing Hyperelatic Large Strain Models, *Computational Mechanics*, 25: 66-77.

Hart, G. and Wong, K. 2000. Structural Dynamics for Structural Engineers, John Wiley and Sons, Inc., New York.

Hwang, J.S., Wu, J.D., Pan, T.C. and Yang, G. 2002. A Mathematical Hysteretic Model for Elastomeric Isolation Bearings, *Earthquake Engineering and Structural Dynamics*, 31: 771-789.

Ogden, R.W. 1984. Nonlinear Elastic Deformations, Ellis Harwood, Chichester,UK.

Saleeb, A.F., Chang, T.Y.P. and Arnold, S.M. 1992. On the Development of Explicit Robust Schemes for Implementations of a Class of Hyperelastic Models in Large-strain Analysis of Rubbers. *Int. J. Numerical Methods in Engineering*, 33: 1237-1249.

Salomon, O., Oller, S. and Barbat, A. 1999. Finite Element Analysis of Base Isolated Buildings Subjected to Earthquake Loads. *International Journal for Numerical Methods in Engineering*, 46: 1741-1761.

UBC, Uniform Building Code. 1997. *International Conference of Building Officials*, Whittier, California.